Stem Cell Reports
Report

ISSCR

OPEN ACCESS

MMP-9 and MMP-2 Contribute to Neuronal Cell Death in iPSC Models of Frontotemporal Dementia with *MAPT* Mutations

Md Helal U. Biswas,[1] Sandra Almeida,[1] Rodrigo Lopez-Gonzalez,[1] Wenjie Mao,[2] Zhijun Zhang,[1,5] Anna Karydas,[3] Michael D. Geschwind,[3] Jacek Biernat,[4] Eva-Maria Mandelkow,[4] Kensuke Futai,[2] Bruce L. Miller,[3] and Fen-Biao Gao[1,*]

[1]Department of Neurology
[2]Department of Psychiatry, Brudnick Neuropsychiatric Research Institute
University of Massachusetts Medical School, Worcester, MA 01605, USA
[3]Department of Neurology, Memory and Aging Center, University of California, San Francisco, San Francisco, CA 94143, USA
[4]German Center for Neurodegenerative Diseases, Ludwig-Erhard-Allee 2, 53175 Bonn, Germany
[5]Present address: Neuroscience and Neuroengineering Research Center, Med-X Research Institute, School of Biomedical Engineering, Shanghai Jiao Tong University, Shanghai 200030, China
*Correspondence: fen-biao.gao@umassmed.edu
http://dx.doi.org/10.1016/j.stemcr.2016.08.006

SUMMARY

How mutations in the microtubule-associated protein tau (*MAPT*) gene cause frontotemporal dementia (FTD) remains poorly understood. We generated and characterized multiple induced pluripotent stem cell (iPSC) lines from patients with *MAPT* IVS10+16 and tau-A152T mutations and a control subject. In cortical neurons differentiated from these and other published iPSC lines, we found that *MAPT* mutations do not affect neuronal differentiation but increase the 4R/3R tau ratio. Patient neurons had significantly higher levels of MMP-9 and MMP-2 and were more sensitive to stress-induced cell death. Inhibitors of MMP-9/MMP-2 protected patient neurons from stress-induced cell death and recombinant MMP-9/MMP-2 were sufficient to decrease neuronal survival. In tau-A152T neurons, inhibition of the ERK pathway decreased MMP-9 expression. Moreover, ectopic expression of 4R but not 3R tau-A152T in HEK293 cells increased MMP-9 expression and ERK phosphorylation. These findings provide insights into the molecular pathogenesis of FTD and suggest a potential therapeutic target for FTD with *MAPT* mutations.

INTRODUCTION

Frontotemporal dementia (FTD), the second most common form of presenile dementia, often causes changes in personality and behavior (Boxer and Miller, 2005). There is no effective treatment, and the molecular pathogenic mechanisms are poorly understood (Roberson, 2012; Irwin et al., 2015). Mutations in the gene encoding the microtubule-associated protein tau (*MAPT*) are responsible for a substantial fraction of FTD cases (Hutton et al., 1998; Loy et al., 2014). Tau pathology is also a hallmark of Alzheimer's disease (AD), and its pathogenic roles and utility as a potential drug target in AD have been extensively investigated (Wang and Mandelkow, 2016; Yoshiyama et al., 2013).

Tau helps assemble and stabilize microtubules. In the CNS, several isoforms of tau are produced from a single gene by alternative splicing (Goedert et al., 1989). More than 40 pathogenic *MAPT* mutations have been described in more than 100 families with FTD (Cruts et al., 2012; Alzheimer Disease & Frontotemporal Dementia Mutation Database, http://www.molgen.vib-ua.be/FTDMutations). Many *MAPT* mutations are either missense mutations or small deletions in the coding region or in introns, which can affect alternative splicing (e.g., of exon 10) (Hutton et al., 1998; Niblock and Gallo, 2012). Tau also modulates signaling cascades by acting as scaffolding proteins for signaling complexes such as FYN, GRB2, and PLCγ, and may also affect other cellular functions (Ittner et al., 2010; Morris et al., 2011).

Many studies of tau toxicity have used cellular or animal models in which wild-type (WT) or mutant tau is ectopically overexpressed (Morris et al., 2011; Wittmann et al., 2001). Patient-specific induced pluripotent stem cells (iPSCs) are an exciting alternative approach to study disease genes in their native genetic context (Yamanaka, 2007) and uncover novel pathogenic mechanisms in AD, Parkinson's disease, FTD, and other neurodegenerative disorders (Israel et al., 2012; Soldner et al., 2009; Almeida et al., 2012). Here we generated and characterized multiple iPSC lines from an FTD patient with a *MAPT* IVS10+16 mutation, an FTD patient with the tau-A152T variant, and a control subject. The *MAPT* IVS10+16 mutation is relatively common and found in many families in different countries (Hutton et al., 1998; Janssen et al., 2002). The tau-A152T variant has been shown to significantly increase the risk for both FTD and AD (Coppola et al., 2012; Kara et al., 2012) and induce aggregation-independent toxicity (Pir et al., 2016). To study their pathogenic mechanisms, we differentiated these newly generated iPSC lines, as well as published control and tau-A152T lines (Almeida et al., 2012; Fong et al., 2013) into postmitotic cortical neurons and identified upregulation of matrix metalloproteinase 9

(MMP-9) through the ERK pathway as an important pathogenic mechanism in FTD with *MAPT* mutations.

RESULTS

Generation of Patient-Specific iPSC Lines with *MAPT* Mutations

To understand how endogenously expressed mutant tau contributes to eventual neurodegeneration, we obtained skin biopsies from two patients with *MAPT* mutations and a healthy control subject. Patient 1 was a male with a tau-A152T variant. The patient's clinical history and neurologic examination were consistent with a diagnosis of progressive supranuclear palsy (PSP). Patient 2 was a male with an *MAPT* IVS10+16 mutation whose clinical diagnosis was largely normal at the time of skin biopsy but developed FTD later on. The control subject is a female family member of patient 2. Putative iPSC lines were derived from the fibroblasts as described previously (Yamanaka, 2007; Almeida et al., 2012), and 10–15 putative iPSC lines from each subject were extensively characterized. Immunocytochemistry analysis showed expression of stem cell makers such as OCT4, SSEA4, NANOG, TRA1-60, and TRA1-81 in all selected iPSC lines (Figure S1A). qRT-PCR showed that total and endogenous expression levels of the four reprogramming factors were the same in each line, confirming silencing of the transgene (Figure S1B). The iPSC lines had normal karyotypes (Figure S1C), and selected lines could differentiate into cell types of all three germ layers, confirming their pluripotency (Figure S1D). Based on these characterizations, we selected iPSC lines 3L1 of control 1, 19L3 and 19L4 of patient 1, and 3L6 and 3L9 of patient 2 for further study. In addition to the lines generated in our current study, we also used two published control iPSC lines, 2L17 and 2L20, derived from a male (Almeida et al., 2012), and one published iPSC line from another tau-A152T mutation male carrier (Fong et al., 2013).

MAPT Mutations Do Not Affect Early Neuronal Differentiation

At passages 25–30, all fully reprogrammed control and patient iPSC lines were differentiated into postmitotic cortical neurons as described (Figure 1A) (Almeida et al., 2012). Four weeks after terminal differentiation, 80% of cells were positive for the neuron-specific marker MAP2, and there was no significant difference between control and patient neurons (Figure S2A). The percentages of VGLUT1-positive excitatory and GABA-positive inhibitory neurons were similar in neuronal cultures differentiated from control and patient iPSCs (Figures S2B and S2C). Moreover, the total expression levels of tau and PSD-95 were the same in 1-month-old neurons derived from control and patient iPSCs (Figure 1B).

To further characterize differentiated human cortical neurons, we performed whole-cell voltage-clamp recordings. Tetrodotoxin-sensitive action potentials were induced in 64% of control neurons, 78% of tau-A152T neurons, and 78% of *MAPT* IVS10+16 neurons (9–11 cells were recorded for each group, Figure 1C). The resting membrane potential did not differ among neurons differentiated from all iPSC lines (Figure S2D). Functional synaptic connections formed in these cell lines, as shown by α-amino-3-hydroxy-5-methyl-4-isoxazole propionate (AMPA)-type glutamate receptor-mediated spontaneous excitatory postsynaptic currents (sEPSCs) that could be blocked with (2,3-dihydroxy-6-nitro-7-sulfamoyl-benzo[f] quinoxaline-2,3-dione (NBQX) (Figure 1D). The mean amplitude, frequency, rise time, and decay time constant of sEPSCs were indistinguishable in all lines (Figures S2E–S2H). Thus, both molecular and electrophysiological analyses suggest *MAPT* mutations do not affect early neuronal differentiation. Therefore, any disease-relevant phenotypes would unlikely be due to changes in neuronal subtypes.

MAPT Mutations Increase the Level and Activity of Secreted MMP-9 and MMP-2

MMPs, a family of Zn-containing proteolytic enzymes, modulate both normal development and human pathophysiology. MMP-9 directly cleaves Huntingtin protein in Huntington's disease, a progressive neurodegenerative disorder (Miller et al., 2010). Moreover, dysregulation of MMP-9 in the CNS is a cause of neuronal developmental disorders (Reinhard et al., 2015). Thus, we set out to examine MMP-9 production in control and patient neurons with *MAPT* mutations. To this end, we performed zymography as described previously (Biswas et al., 2010), which measures the level and total activity of MMP-9. Tau-A152T neurons had >10-fold higher level and activity of secreted MMP-9 than control neurons (Figures 2A and 2B), as did *MAPT* IVS10+16 neurons to a lesser extent (Figures 2C and 2D). The total activity of secreted MMP-2 was more than 2-fold higher in patient-specific neurons than in controls (Figures 2A–2D). The level of secreted MMP-9 and MMP-2 was also increased in cortical neurons derived from a published iPSC line with the tau-A152T mutation (Fong et al., 2013) (Figures 2E and 2F). The effect on the total level and activity of secreted MMP-9/MMP-2 seems to be specific to mutant tau, since in progranulin-deficient FTD cortical neurons, there was no significant change in secreted MMP-2 level (Figure S2I) and the secreted MMP-9 level was below detection as in control neurons (not shown). This increase is likely in part due to transcriptional regulation, since the mRNA levels of *MMP-9* and *MMP-2* in tau-A152T and *MAPT* IVS10+16 neurons were higher than in control neurons (Figure S2J).

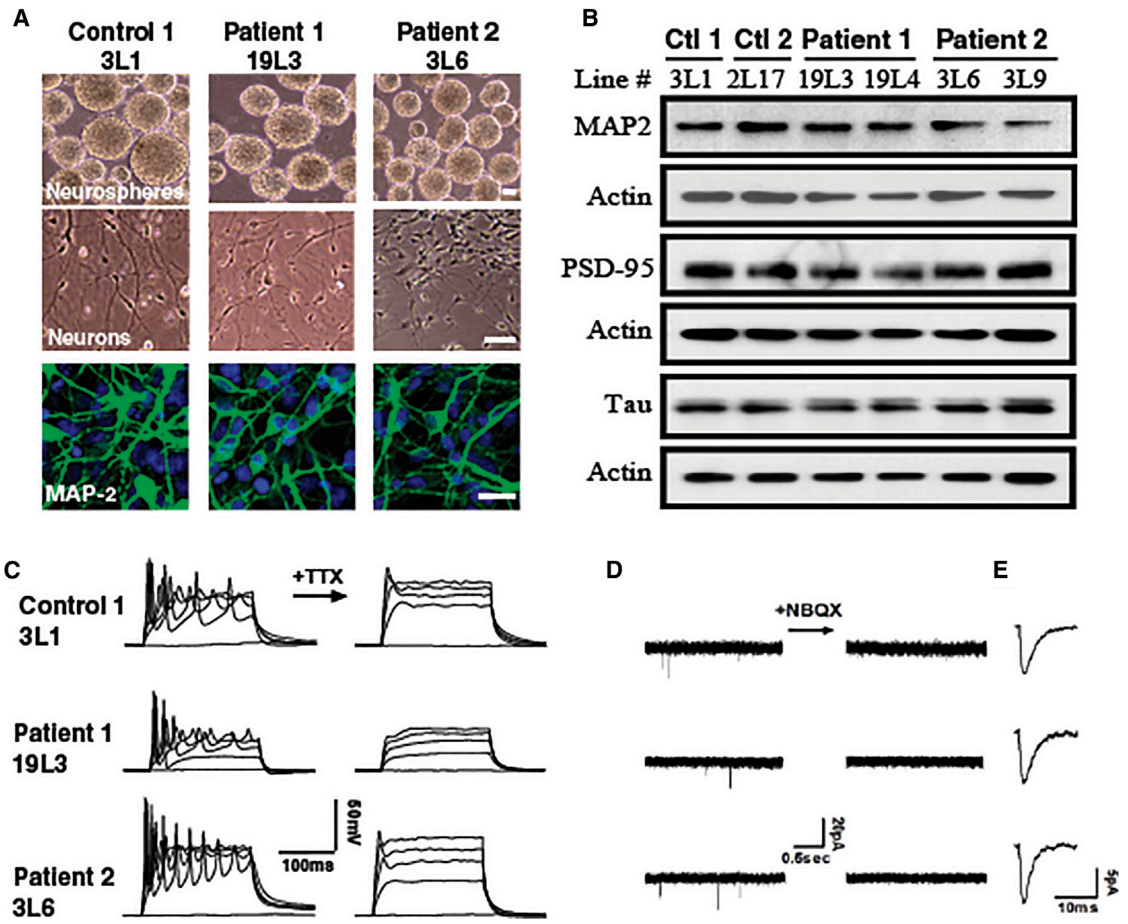

Figure 1. Differentiation and Characterization of Cortical Neurons Derived from iPSC Lines from FTD Patients and Control Subjects

(A) Phase-contrast images of neurospheres (upper), differentiated neurons (middle), and MAP-2 immunostaining of neurons (lower) from the iPSC lines. Scale bars, 50 μm.

(B) Western blot analysis of MAP-2, PSD-95, and tau-expression levels in 4-week-old neurons differentiated from iPSC lines. Actin served as the loading control.

(C) Representative action potentials elicited by current injection (0–400 pA in 100-pA steps) and blocked by tetrodotoxin (TTX) of lines 3L1 of control 1, 19L3 of patient 1, and 3L6 of patient 2. Nine to eleven cells were recorded for each group.

(D) iPSC-derived neurons (n = 7 per subject) displayed synaptic responses and were sensitive to the AMPA receptor antagonist NBQX.

(E) Averaged sEPSC events from neurons of different subjects.

See also Figures S1 and S2.

Elevated Extracellular MMP-9 and MMP-2 Contribute to Neuronal Cell Death of iPSC-Derived Human Cortical Neurons with *MAPT* Mutations

The increased extracellular MMP-9 and MMP-2 activity in FTD patient-specific cortical neurons suggests that these molecular changes may contribute to disease phenotypes. To investigate this possibility, we first examined the relative survival of human cortical neurons derived from control subjects of patients with *MAPT* mutations without any inducers of cellular stress. We found that, indeed, $TUJ1^+$ neurons showed reduced survival as measured by TUNEL analysis (Figure 3A). Interestingly, we did not observe TUNEL labeling in more than 100 glial cells (Figure S3A), suggesting glial cells are less vulnerable to increased MMP-9 and MMP-2 levels. We then examined the sensitivity of iPSC-derived human cortical neurons to different inducers of cellular stress. We treated these neurons with staurosporine, a broad-spectrum kinase inhibitor that induces apoptosis (Budd et al., 2000); rotenone, a complex I inhibitor that induces mitochondrial dysfunction (Sherer et al., 2003); and rapamycin, an inhibitor of the mammalian target of the rapamycin (mTOR) signaling pathway with many downstream effects (Li et al., 2014). When measuring cell viability using the MTT assay, we found

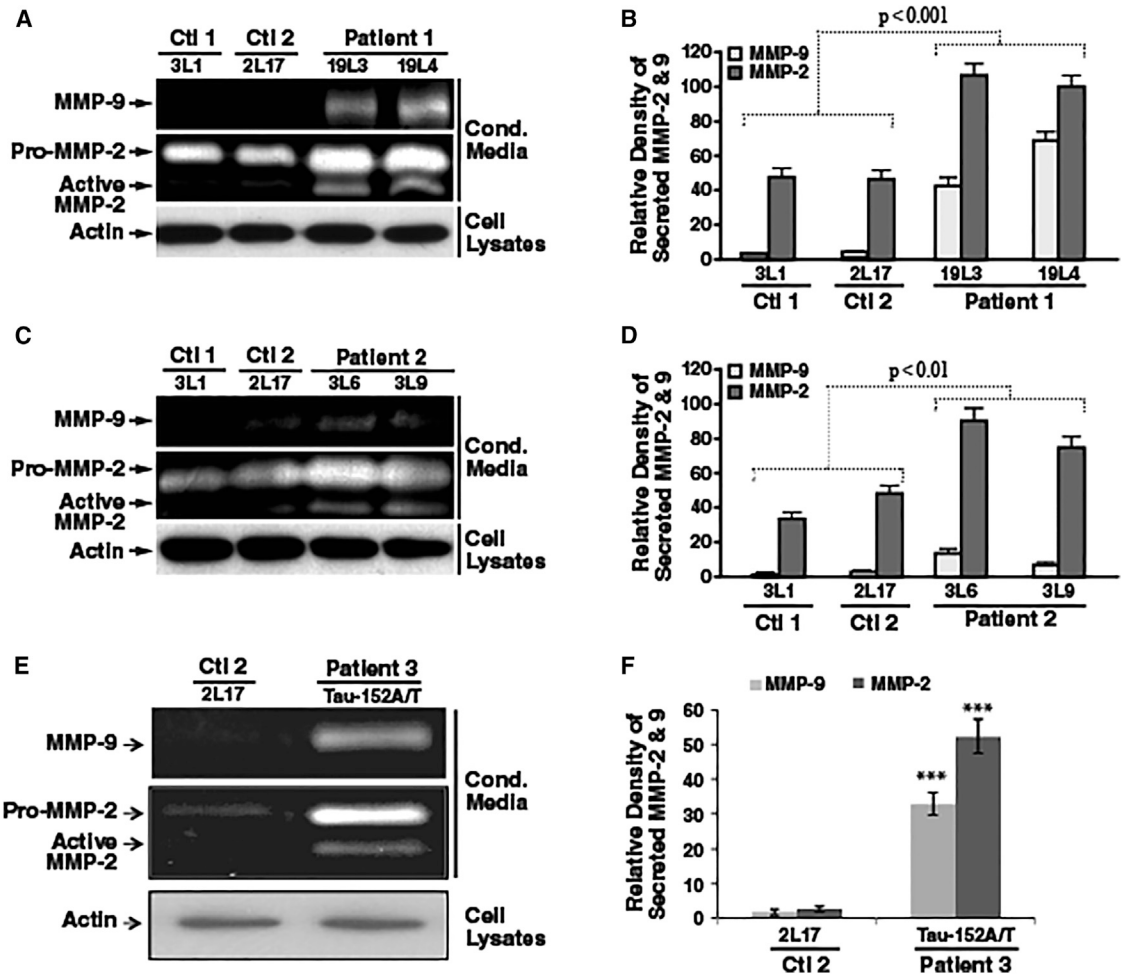

Figure 2. MMP-9 and MMP-2 Expression Is Increased in Human Neurons with *MAPT* Mutations

(A) Zymographic analysis of secreted MMP-9 and MMP-2 in conditioned media from tau-A152T human neurons (patient 1). Immunoblotting of cell lysates with actin served as the loading control.

(B) Quantification of secreted MMP-9 and MMP-2 in (A). Values are mean ± SD of three independent experiments. $p < 0.001$ by Student's t test.

(C) Zymographic analysis of the level of secreted MMP-9 and MMP-2 in conditioned media from *MAPT* IVS10+16 human neurons (patient 2). Immunoblotting of cell lysates with actin served as the loading control.

(D) Quantification of secreted MMP-9 and MMP-2 in C. Values are mean ± SD of three independent experiments. $p < 0.01$ by Student's t test.

(E) Zymographic analysis for MMP-9 and MMP-2 in conditioned media from tau-A152T human neurons (patient 3; Fong et al., 2013). Immunoblotting of cell lysates with actin served as the loading control.

(F) Quantification of MMP-2 and MMP-9 levels in (E) based on three experiments. Values are mean ± SD of three experiments. ***$p < 0.001$ by Student's t test.

See also Figure S3.

that patient-specific neurons are more sensitive than control neurons to cell death induced by rapamycin (Figure 3B) but not by staurosporine or rotenone (Figures S3B and S3C), suggesting compromised function in the mTOR pathway or related molecular pathways. For this experiment, we compared relative survival of neurons derived from the same iPSC line with or without the treatment with inducers of cellular stress; thus, the value from the MTT assay without stressors for each line was always taken as 100%.

To examine the contribution of MMP-9 and MMP-2 to reduced survival of iPSC-derived cortical neurons with *MAPT* mutations, we quantified their mRNA levels in iPSC-derived 4-week-old human neurons treated with rapamycin for an additional 3 days. *MMP-9*/*MMP-2* mRNA levels in tau-A152T and *MAPT* IVS10+16 neurons were

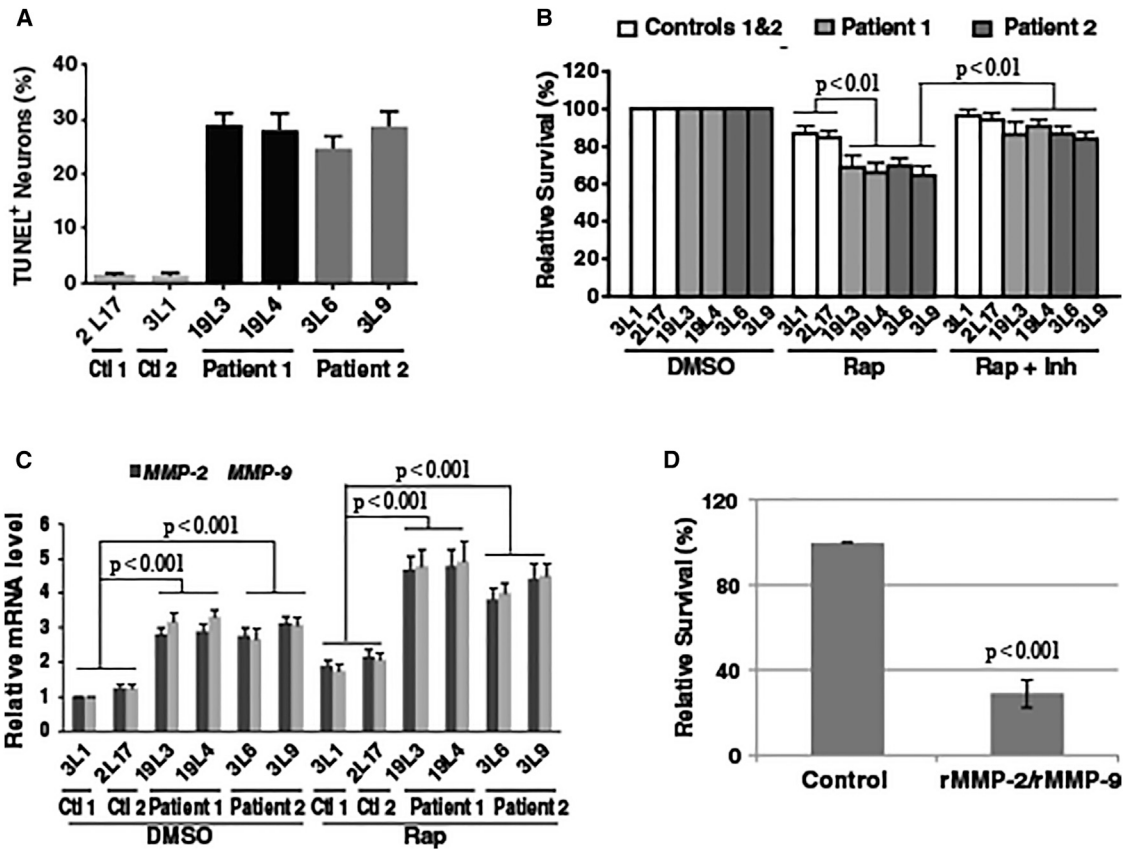

Figure 3. Increased MMP-9 and MMP-2 Expression Contributes to Neurodegeneration of Patient Neurons under Stress

(A) TUNEL analysis of TUJ1$^+$ 4-week-old cortical neurons from controls and tau patients under basal conditions. Values are mean ± SD of two independent experiments and in each experiment, 100 cells were counted for each iPSC line.

(B) Percentage of human neuron survival after 48 hr of treatment with DMSO, 40 nM rapamycin, or 40 nM rapamycin and inhibitors (Inh) of MMP-2 (5 μM) and MMP-9 (200 nM). Values are mean ± SD from three independent experiments.

(C) qRT-PCR analysis of *MMP-2* and *MMP-9* mRNA levels in human neurons after treatment with DMSO or 40 nM rapamycin (Rap). Values are mean ± SD from three independent experiments.

(D) Survival of 4-week-old control human neurons 48 hr after treatment with recombinant MMP-2 (5 μg/mL) and MMP-9 (5 μg/mL). Values are mean ± SD of three independent experiments.

Statistical significance is indicated by p values and was determined by Student's t test. See also Figure S3.

significantly higher than that in control neurons (Figure S2J), and rapamycin increased these levels ($p < 0.01$) (Figure 3C). Human neurons differentiated from iPSCs are difficult to transfect at high efficiency. To examine the contributions of increased MMP-9 and MMP-2 to neuronal cell death, we used two compounds that are known to inhibit MMP-9 and MMP-2 activity (catalog #444278 and #444244, Calbiochem). We found that this treatment partially rescued the increased sensitivity to rapamycin and improved survival (Figure 3B). Furthermore, treatment with recombinant MMP-9/MMP-2 induced neuronal cell death in 4-weeek-old postmitotic cortical neurons differentiated from iPSCs of a healthy control subject, as measured by MTT assay (Figure 3D). MMP-2 and MMP-9 seem to induce cell death directly, since this treatment also increased the TUNEL signal in iPSC-derived neurons (Figures S3D and S3E). These results suggest that elevated extracellular MMP-9 and MMP-2 are sufficient to cause neuronal cell death in human neurons. Taken together, our data suggest that elevated level and activity of extracellular MMP-9 and MMP-2 are in part responsible for the observed loss of patient neurons under rapamycin-induced stress.

4R Tau-A152T Activates the ERK Pathway to Increase MMP-9 Expression

It is known that MMP-9 expression is regulated by ERK (Wang et al., 2006). Therefore, to explore the mechanism by which mutant tau increases MMP-9 production in iPSC-derived patient neurons with *MAPT* mutations, we

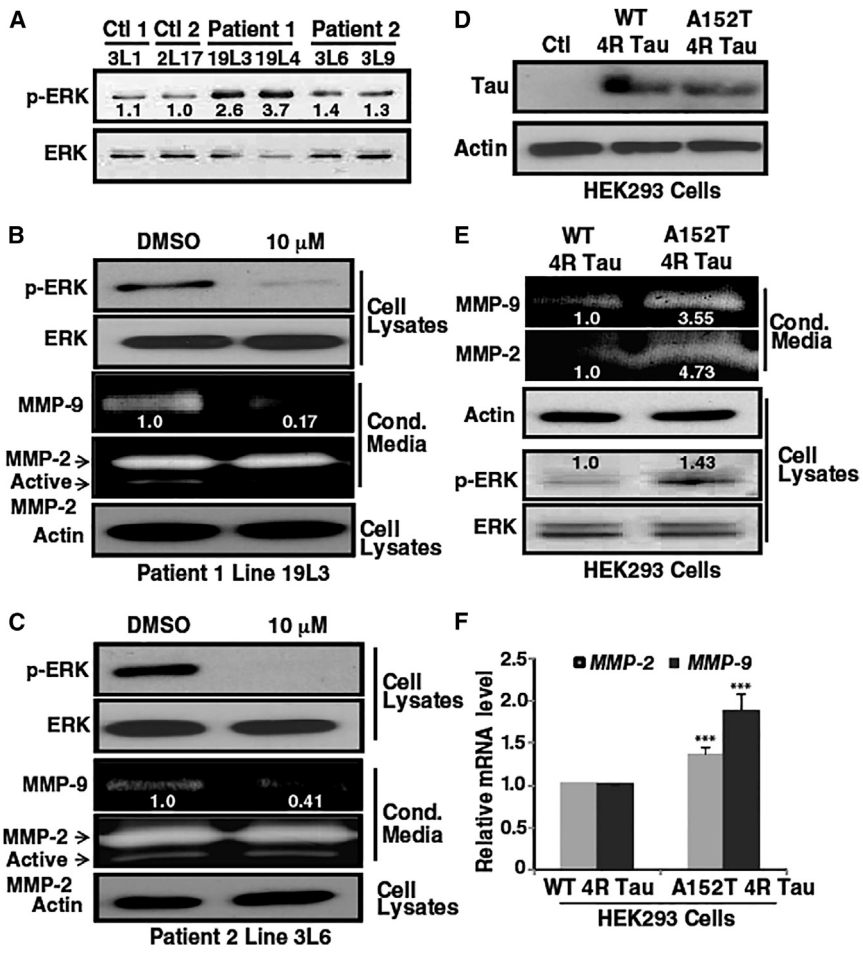

Figure 4. The tau-A152T Mutation Increases MMP-9 Expression through Effects on ERK

(A) Western blot analysis of ERK and p-ERK in 4-week-old iPSC-derived human cortical neurons.

(B and C) Neurons from line 3 of patient 1 (B) and line 6 of patient 2 (C) were treated with DMSO or the MEK inhibitor PD98059. Cell lysates were analyzed by western blot with antibodies against p-ERK, ERK, and actin, and conditioned media were analyzed by zymography for MMP-9 and MMP-2. The numbers indicate the levels of MMP-9 relative to actin.

(D) Western blot analysis of tau levels in HEK293 cells transfected with human 4R WT or 4R tau-A152T.

(E) Zymographic analysis of secreted MMP-9 and MMP-2 in conditioned media, and western blot analysis of actin, p-ERK, and ERK levels in respective lysates from HEK293 cells expressing 4R WT or 4R tau-A152T.

(F) qRT-PCR analysis of the expression levels of *MMP-2* and *MMP-9* mRNA in HEK293 cells expressing 4R WT or 4R tau-A152T. Values are mean ± SD from three independent experiments. ***p < 0.001 by Student's t test.

first examined ERK-pathway activity. The level of phosphorylated ERK (p-ERK) was significantly increased in tau-A152T neurons and to a lesser extent in *MAPT* IVS10+16 patient neurons (Figure 4A). It is worth noting that the level and activity of secreted MMP-9 in tau-A152T neurons is also substantially higher than that in *MAPT* IVS10+16 neurons (Figure 2). ERK phosphorylation in *MAPT* mutant neurons was blocked by treatment with PD98059, a specific inhibitor of MEK-mediated activation of ERK (Li et al., 2001) (Figures 4B and 4C). Correspondingly, the level and activity of secreted MMP-9 was greatly suppressed in both tau-A152T and *MAPT* IVS10+16 patient neurons (Figures 4B and 4C), suggesting that MMP-9 expression is regulated by the ERK signaling pathway in cortical neurons. To further confirm the regulation of MMP-9 by ERK activation, we treated cortical neurons of both patient 1 and patient 2 with lower concentrations of PD98059. We found the level and activity of secreted MMP-9 to correlate well with the extent of ERK phosphorylation (Figure S4A). Interestingly, the level and activity of MMP-2 was not affected after the PD98059 treatment in tau-A152T neurons (Figure 4B) and *MAPT* IVS10+16 neurons (Figure 4C). These results suggest that FTD-causing *MAPT* mutations increase MMP-9 through ERK activation, while the molecular regulation of MMP-2 induction in patient neurons remains to be identified.

To further confirm the role of mutant tau in MMP-9 production, we first examined the 4R/3R tau ratio in iPSC-derived patient neurons. As expected, the 4R/3R tau ratio is greatly increased in *MAPT* IVS10+16 neurons (Figure S3F) but not in *GRN* mutant neurons (Figure S3G). Interestingly, this ratio is also increased, but to a lesser extent, in tau-A152T neurons (Figure S3F). We then transfected HEK293 cells, which do not normally express tau, with either 3R or 4R WT tau or tau-A152T. 4R WT and 4R tau-A152T were expressed at comparable levels, as shown by western blot (Figure 4D). However, the secreted MMP-9 level and activity in conditioned medium was significantly higher in cultures of cells expressing tau-A152T than WT tau (Figure 4E). The *MMP-9* mRNA level was also higher in cells expressing tau-A152T (Figure 4F). Correspondingly, the level of p-ERK was also elevated in HEK293 cells expressing

tau-A152T (Figure 4E). Interestingly, the level and activity of secreted MMP-9 in HEK293 cells expressing WT 3R tau and 3R tau-A152T are similar (Figures S4B and S4C). ERK phosphorylation is also not affected by A152T mutation in 3R tau (Figure S4D). Taken together, these findings strongly suggest that 4R tau-A152T activates the ERK pathway more strongly, which in turn increases the level and activity of secreted MMP-9. 4R tau-A152T expression (Figures 4E and 4F) but not inhibition of ERK activity (Figures 4B and 4C) also increases the total activity of secreted MMP-2, suggesting that tau-A152T increases the level and activity of secreted MMP-2, likely through an ERK-independent pathway.

DISCUSSION

In this study, we found a significant increase in the level and activity of secreted MMP-9 and MMP-2 in cortical neurons derived from iPSCs of three subjects with *MAPT* mutations. More importantly, this increase contributed to neuronal cell loss induced by cellular stress, and inhibition of MMP-9/MMP-2 activity was neuroprotective. Our results are consistent with a recent paper published during our study in which the authors showed that MMP-9 is specifically expressed in fast motor neurons and contributes to selective neuronal vulnerability in amyotrophic lateral sclerosis (ALS) (Kaplan et al., 2014). Moreover, reduction of MMP-9 through genetic or pharmacological approaches delayed muscle denervation in vivo (Kaplan et al., 2014). Thus, MMP-9 is a potential therapeutic target for both FTD and ALS, although how MMP-9 induces cell death in iPSC-derived cortical neurons remains to be determined at a mechanistic level.

Our studies also provide mechanistic insight into the increased level and activity of secreted MMP-9 in cortical neurons derived from FTD patient-specific iPSCs with *MAPT* mutations. The increase seems to be mediated by ERK-pathway activation. Indeed, ectopic expression of mutant 4R but not 3R tau in HEK293 cells resulted in ERK phosphorylation and increased MMP-9 production. However, the molecular pathways of MMP-2 induction remain to be further delineated. These results further support the notion that tau is not only a key substrate for phosphorylation but also functions upstream of several kinase signaling pathways (Ittner et al., 2010; Morris et al., 2011; Vossel et al., 2015). Our iPSC lines with different *MAPT* mutations will be useful for further investigations of the roles of endogenous tau in cell signaling and neuronal vulnerability, such as in an accompanying paper by Silva et al. (2016). In the future, it will be useful to generate isogenic iPSC lines with different *MAPT* mutations and confirm the effect of endogenous mutant tau on the ERK-MMP-9 pathway. Moreover, since different tau strains with prion-like properties cause different tauopathies in vitro and in vivo (Sanders et al., 2014), it will be also interesting to determine which tau strains are present in iPSC-derived human neurons and activate the ERK pathway.

EXPERIMENTAL PROCEDURES

Isolation of Primary Human Skin Fibroblasts and Generation of iPSCs

Skin biopsies were obtained from two patients with *MAPT* mutation. Patient 1 was a 68-year-old man with a 6-year history of personality changes and cognitive and speech deterioration. He was diagnosed with PSP and has a tau-A152T mutation. Patient 2 was presymptomatic at the time of skin biopsy but had an extensive family history of FTD and has a *MAPT* IVS10+16 mutation.

iPSCs were generated as described by Almeida et al. (2012). In brief, fibroblasts were transduced for 7 days with equal volumes of supernatant from retroviruses expressing human *OCT3/4*, *SOX2*, *KLF4*, and *c-MYC* and seeded onto mitomycin C-treated SNL feeder cells. Five weeks after viral transduction, individual colonies were picked and transferred to 12-well plates containing feeder cells for expansion. Well-established iPSC lines were adapted to feeder-free conditions and maintained with mTeSR1 medium (STEMCELL Technologies) on Matrigel (BD Biosciences).

SUPPLEMENTAL INFORMATION

Supplemental Information includes Supplemental Experimental Procedures and four figures and can be found with this article online at http://dx.doi.org/10.1016/j.stemcr.2016.08.006.

AUTHOR CONTRIBUTIONS

B.L.M. and F.B.G. initiated the project. M.H.U.B., S.A., and F.-B.G. designed the studies, analyzed the data, and wrote the manuscript. M.H.U.B. did most of the experiments. Z.Z. helped S.A. with iPSC generation. R.L.-G. differentiated some iPSC lines and performed TUNEL assays. W.M. and K.F. conducted the electrophysiological analysis. A.K., M.D.G., and B.L.M. provided patient skin biopsies. J.B. and E.-M.M. generated tau-expression vectors. F.B.G. supervised the project.

ACKNOWLEDGMENTS

We thank patients and their families for their generosity. We also thank S. Ordway and Gao laboratory members for comments, and Y. Huang for providing one published tau-152A/T iPSC line. This work is supported by the Tau Consortium (F.B.G., B.L.M., E.M.M.), the Whitehall Foundation (2012-08-44 to K.F.), and the NIH (NS057553 and NS079725 to F.B.G.; AG019724 and AG023501 to B.L.M.).

Received: February 18, 2016
Revised: August 9, 2016
Accepted: August 11, 2016
Published: September 1, 2016

REFERENCES

Almeida, S., Zhang, Z., Coppola, G., Mao, W., Futai, K., Karydas, A., Geschwind, M.D., Tartaglia, M.C., Gao, F., Gianni, D., et al. (2012). Induced pluripotent stem cell models of progranulin-deficient frontotemporal dementia uncover specific reversible neuronal defects. Cell Rep. *2*, 789–798.

Biswas, M.H., Du, C., Zhang, C., Straubhaar, J., Languino, L.R., and Balaji, K.C. (2010). Protein kinase D1 inhibits cell proliferation through matrix metalloproteinase-2 and matrix metalloproteinase-9 secretion in prostate cancer. Cancer Res. *70*, 2095–2104.

Boxer, A.L., and Miller, B.L. (2005). Clinical features of frontotemporal dementia. Alzheimer Dis. Assoc. Disord. *19*, S3–S6.

Budd, S.L., Tenneti, L., Lishnak, T., and Lipton, S.A. (2000). Mitochondrial and extramitochondrial apoptotic signaling pathways in cerebrocortical neurons. Proc. Natl. Acad. Sci. USA *97*, 6161–6166.

Coppola, G., Chinnathambi, S., Lee, J.J., Dombroski, B.A., Baker, M.C., Soto-Ortolaza, A.I., Lee, S.E., Klein, E., Huang, A.Y., Sears, R., et al. (2012). Evidence for a role of the rare tau-A152T variant in MAPT in increasing the risk for FTD-spectrum and Alzheimer's diseases. Hum. Mol. Genet. *21*, 3500–3512.

Cruts, M., Theuns, J., and Van Broeckhoven, C. (2012). Locus-specific mutation databases for neurodegenerative brain diseases. Hum. Mutat. *33*, 1340–1344.

Fong, H., Wang, C., Knoferle, J., Walker, D., Balestra, M.E., Tong, L.M., Leung, L., Ring, K.L., Seeley, W.W., Karydas, A., et al. (2013). Genetic correction of tauopathy phenotypes in neurons derived from human induced pluripotent stem cells. Stem Cell Rep. *1*, 226–234.

Goedert, M., Spillantini, M.G., Jakes, R., Rutherford, D., and Crowther, R.A. (1989). Multiple isoforms of human microtubule-associated protein tau: sequences and localization in neurofibrillary tangles in Alzheimer's disease. Neuron *3*, 519–526.

Hutton, M., Lendon, C.L., Rizzu, P., Baker, M., Froelich, S., Houlden, H., Pickering-Brown, S., Chakraverty, S., Isaacs, A., Grover, A., et al. (1998). Association of missense and 5′-splice-site mutations in tau with the inherited dementia FTDP-17. Nature *393*, 702–705.

Irwin, D.J., Cairns, N.J., Grossman, M., McMillan, C.T., Lee, E.B., Van Deerlin, V.M., Lee, V.M., and Trojanowski, J.Q. (2015). Frontotemporal lobar degeneration: defining phenotypic diversity through personalized medicine. Acta Neuropathol. *129*, 469–491.

Israel, M.A., Yuan, S.H., Bardy, C., Reyna, S.M., Mu, Y., Herrera, C., Hefferan, M.P., Van Gorp, S., Nazor, K.L., Boscolo, F.S., et al. (2012). Probing sporadic and familial Alzheimer's disease using induced pluripotent stem cells. Nature *482*, 216–220.

Ittner, L.M., Ke, Y.D., Delerue, F., Bi, M., Gladbach, A., van Eersel, J., Wölfing, H., Chieng, B.C., Christie, M.J., Napier, I.A., et al. (2010). Dendritic function of tau mediates amyloid-beta toxicity in Alzheimer's disease mouse models. Cell *142*, 387–397.

Janssen, J.C., Warrington, E.K., Morris, H.R., Lantos, P., Brown, J., Revesz, T., Wood, N., Khan, M.N., Cipolotti, L., Fox, N.C., and Rossor, M.N. (2002). Clinical features of frontotemporal dementia due to the intronic tau 10(+16) mutation. Neurology *58*, 1161–1168.

Kaplan, A., Spiller, K.J., Towne, C., Kanning, K.C., Choe, G.T., Geber, A., Akay, T., Aebischer, P., and Henderson, C.E. (2014). Neuronal matrix metalloproteinase-9 is a determinant of selective neurodegeneration. Neuron *81*, 333–348.

Kara, E., Ling, H., Pittman, A.M., Shaw, K., de Silva, R., Simone, R., Holton, J.L., Warren, J.D., Rohrer, J.D., Xiromerisiou, G., et al. (2012). The MAPT tau-A152T variant is a risk factor associated with tauopathies with atypical clinical and neuropathological features. Neurobiol. Aging *33*, 2231.e7–2231.e14.

Li, B.S., Ma, W., Zhang, L., Barker, J.L., Stenger, D.A., and Pant, H.C. (2001). Activation of phosphatidylinositol-3 kinase (PI-3K) and extracellular regulated kinases (ERK1/2) is involved in muscarinic receptor-mediated DNA synthesis in neural progenitor cells. J. Neurosci. *21*, 1569–1579.

Li, J., Kim, S.G., and Blenis, J. (2014). Rapamycin: one drug, many effects. Cell Metab. *19*, 373–379.

Loy, C.T., Schofield, P.R., Turner, A.M., and Kwok, J.B. (2014). Genetics of dementia. Lancet *383*, 828–840.

Miller, J.P., Holcomb, J., Al-Ramahi, I., de Haro, M., Gafni, J., Zhang, N., Kim, E., Sanhueza, M., Torcassi, C., Kwak, S., et al. (2010). Matrix metalloproteinases are modifiers of huntingtin proteolysis and toxicity in Huntington's disease. Neuron *67*, 199–212.

Morris, M., Maeda, S., Vossel, K., and Mucke, L. (2011). The many faces of tau. Neuron *70*, 410–426.

Niblock, M., and Gallo, J.M. (2012). Tau alternative splicing in familial and sporadic tauopathies. Biochem. Soc. Trans. *40*, 677–680.

Pir, G.J., Choudhary, B., Mandelkow, E., and Mandelkow, E.M. (2016). Tau mutant A152T, a risk factor for FTD/PSP, induces neuronal dysfunction and reduced lifespan independently of aggregation in a *C. elegans* tauopathy model. Mol. Neurodegener. *11*, 33.

Reinhard, S.M., Razak, K., and Ethell, I.M. (2015). A delicate balance: role of MMP-9 in brain development and pathophysiology of neurodevelopmental disorders. Front. Cell Neurosci. *9*, 280.

Roberson, E.D. (2012). Mouse models of frontotemporal dementia. Ann. Neurol. *72*, 837–849.

Sanders, D.W., Kaufman, S.K., DeVos, S.L., Sharma, A.M., Mirbaha, H., Li, A., Barker, S.J., Foley, A.C., Thorpe, J.R., Serpell, L.C., et al. (2014). Distinct tau prion strains propagate in cells and mice and define different tauopathies. Neuron *82*, 1271–1288.

Sherer, T.B., Betarbet, R., Testa, C.M., Seo, B.B., Richardson, J.R., Kim, J.H., Miller, G.W., Yagi, T., Matsuno-Yagi, A., and Greenamyre, J.T. (2003). Mechanism of toxicity in rotenone models of Parkinson's disease. J. Neurosci. *23*, 10756–10764.

Silva, M.C., Cheng, C., Mair, W., Almeida, S., Fong, H., Biswas, M.H., Zhang, Z., Temple, S., Coppola, G., Geschwind, D.H., et al. (2016). Human iPSC-derived neuronal model of Tau-A152T frontotemporal dementia reveals Tau-mediated mechanisms of neuronal vulnerability. Stem Cell Rep. *7*, this issue, 325–340.

Soldner, F., Hockemeyer, D., Beard, C., Gao, Q., Bell, G.W., Cook, E.G., Hargus, G., Blak, A., Cooper, O., Mitalipova, M., et al. (2009). Parkinson's disease patient-derived induced pluripotent stem cells free of viral reprogramming factors. Cell *136*, 964–977.

Vossel, K.A., Xu, J.C., Fomenko, V., Miyamoto, T., Suberbielle, E., Knox, J.A., Ho, K., Kim, D.H., Yu, G.Q., and Mucke, L. (2015).

Tau reduction prevents Aβ-induced axonal transport deficits by blocking activation of GSK3β. J. Cell Biol. *209*, 419–433.

Wang, Y., and Mandelkow, E. (2016). Tau in physiology and pathology. Nat. Rev. Neurosci. *17*, 22–35.

Wang, L., Zhang, Z.G., Zhang, R.L., Gregg, S.R., Hozeska-Solgot, A., LeTourneau, Y., Wang, Y., and Chopp, M. (2006). Matrix metalloproteinase 2 (MMP2) and MMP9 secreted by erythropoietin-activated endothelial cells promote neural progenitor cell migration. J. Neurosci. *26*, 5996–6003.

Wittmann, C.W., Wszolek, M.F., Shulman, J.M., Salvaterra, P.M., Lewis, J., Hutton, M., and Feany, M.B. (2001). Tauopathy in *Drosophila*: neurodegenerative without neurofibrillary tangles. Science *293*, 711–714.

Yamanaka, S. (2007). Strategies and new developments in the generation of patient-specific pluripotent stem cells. Cell Stem Cell *1*, 39–49.

Yoshiyama, Y., Lee, V.M., and Trojanowski, J.Q. (2013). Therapeutic strategies for tau mediated neurodegeneration. J. Neurol. Neurosurg. Psychiatry *84*, 784–795.

Stem Cell Reports, Volume *7*

Supplemental Information

MMP-9 and MMP-2 Contribute to Neuronal Cell Death in iPSC Models of Frontotemporal Dementia with *MAPT* Mutations

Md Helal U. Biswas, Sandra Almeida, Rodrigo Lopez-Gonzalez, Wenjie Mao, Zhijun Zhang, Anna Karydas, Michael D. Geschwind, Jacek Biernat, Eva-Maria Mandelkow, Kensuke Futai, Bruce L. Miller, and Fen-Biao Gao

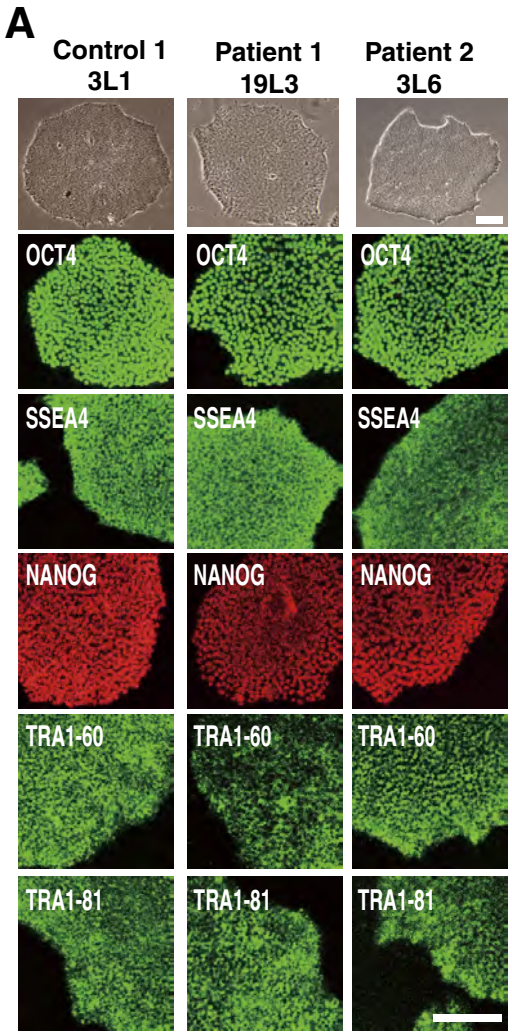
A
Control 1
3L1
Patient 1
19L3
Patient 2
3L6
OCT4
SSEA4
NANOG
TRA1-60
TRA1-81

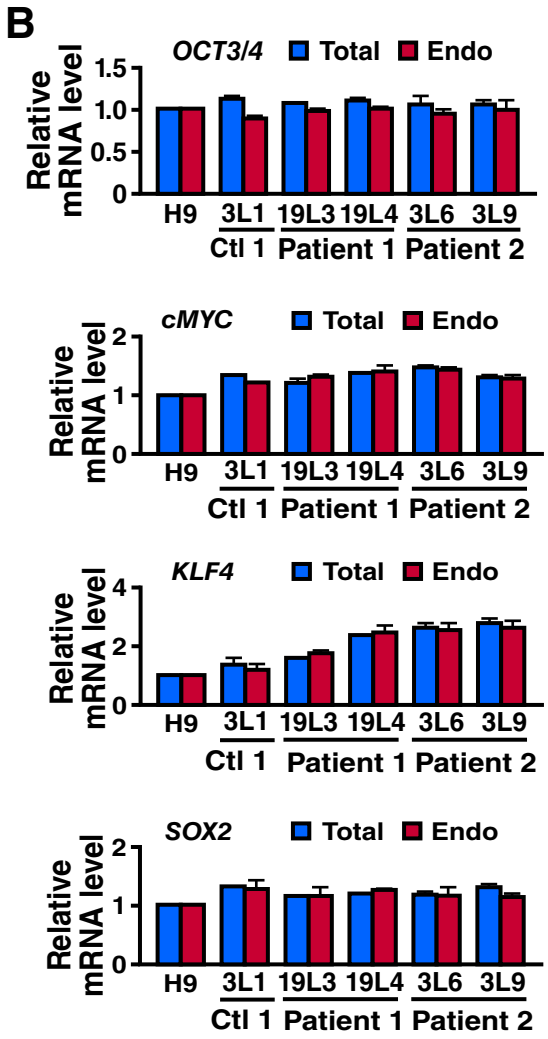
B
OCT3/4
cMYC
KLF4
SOX2
Total
Endo
Relative mRNA level
H9
3L1
19L3
19L4
3L6
3L9
Ctl 1
Patient 1
Patient 2

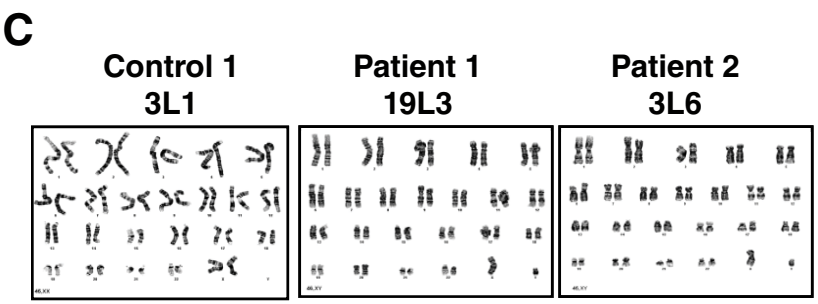
C
Control 1
3L1
Patient 1
19L3
Patient 2
3L6

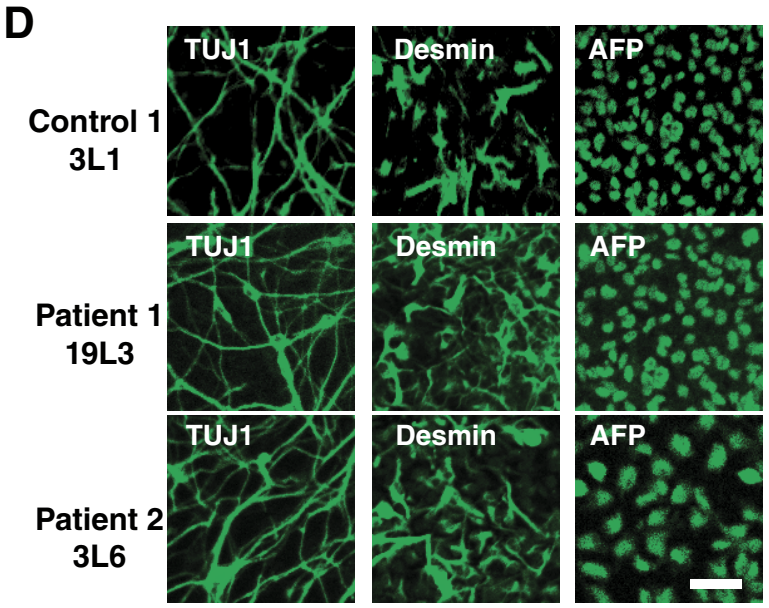
D
Control 1
3L1
Patient 1
19L3
Patient 2
3L6
TUJ1
Desmin
AFP

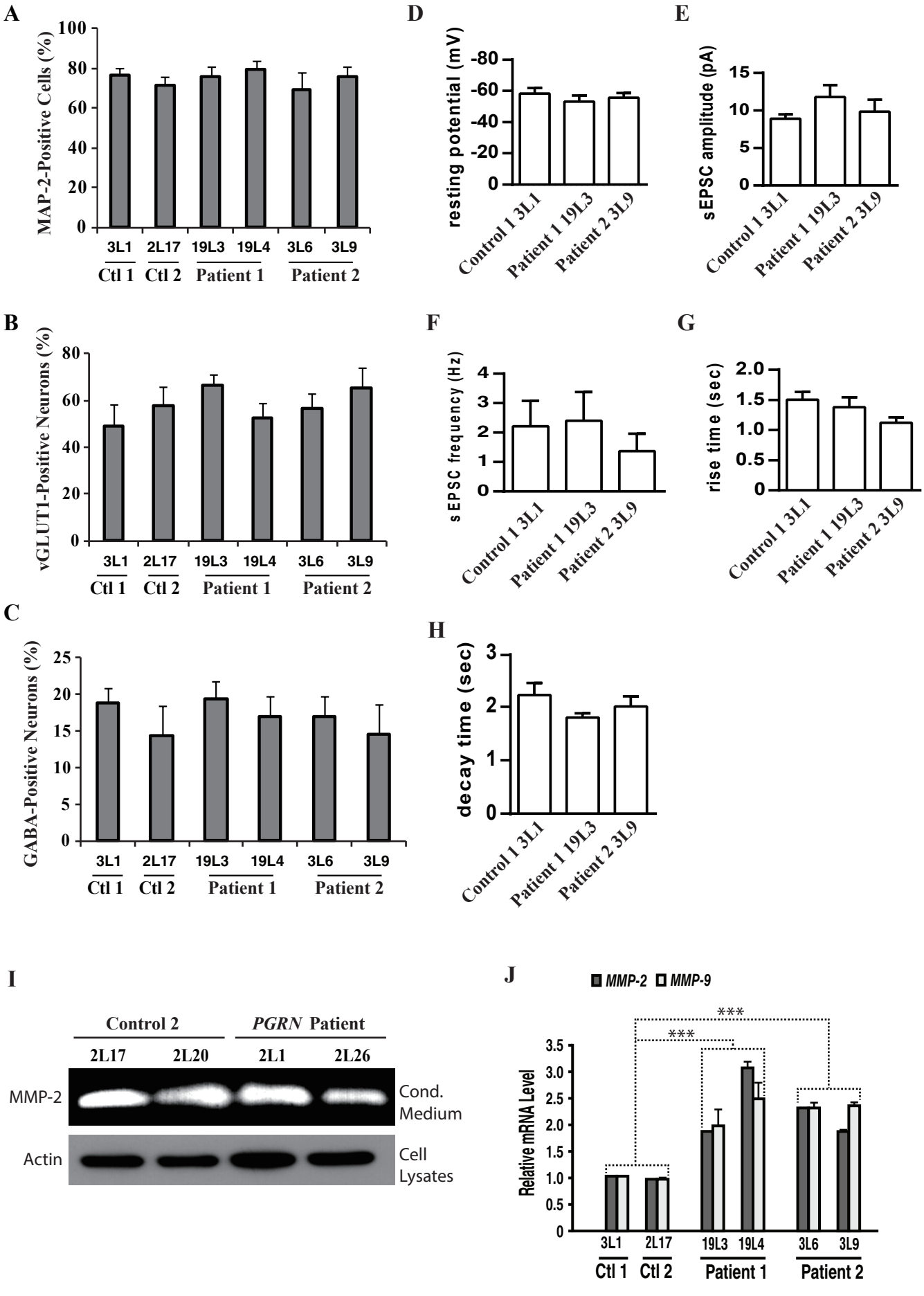
A
MAP-2-Positive Cells (%)
100
80
60
40
20
0
3L1
2L17
19L3
19L4
3L6
3L9
Ctl 1
Ctl 2
Patient 1
Patient 2
B
vGLUT1-Positive Neurons (%)
80
60
40
20
0
C
GABA-Positive Neurons (%)
25
20
15
10
5
0
D
resting potential (mV)
-80
-60
-40
-20
0
Control 1 3L1
Patient 1 19L3
Patient 2 3L9
E
sEPSC amplitude (pA)
15
10
5
0
F
sEPSC frequency (Hz)
4
3
2
1
0
G
rise time (sec)
2.0
1.5
1.0
0.5
0
H
decay time (sec)
3
2
1
0
I
Control 2
PGRN Patient
2L17
2L20
2L1
2L26
MMP-2
Cond. Medium
Actin
Cell Lysates
J
MMP-2
MMP-9
***
***
Relative mRNA Level
3.5
3.0
2.5
2.0
1.5
1.0
0.5
0

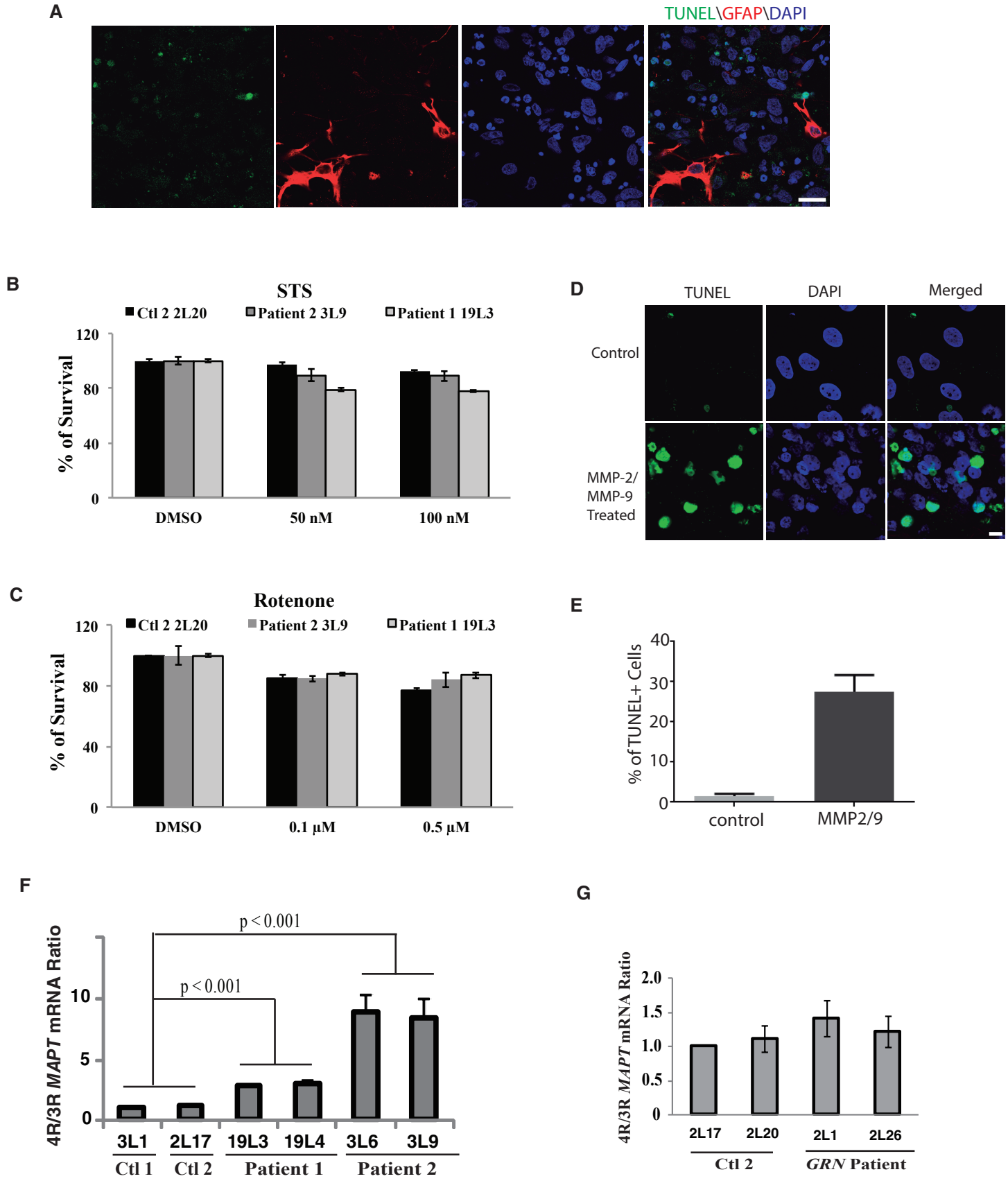
A
TUNEL\GFAP\DAPI
B
STS
Ctl 2 2L20
Patient 2 3L9
Patient 1 19L3
% of Survival
120
80
40
0
DMSO
50 nM
100 nM
C
Rotenone
Ctl 2 2L20
Patient 2 3L9
Patient 1 19L3
% of Survival
120
80
40
0
DMSO
0.1 µM
0.5 µM
D
TUNEL
DAPI
Merged
Control
MMP-2/
MMP-9
Treated
E
% of TUNEL+ Cells
40
30
20
10
0
control
MMP2/9
F
4R/3R MAPT mRNA Ratio
p < 0.001
p < 0.001
10
5
0
3L1
2L17
19L3
19L4
3L6
3L9
Ctl 1
Ctl 2
Patient 1
Patient 2
G
4R/3R MAPT mRNA Ratio
2.0
1.5
1.0
0.5
0
2L17
2L20
2L1
2L26
Ctl 2
GRN Patient

Biswas *et al*, Figure S4

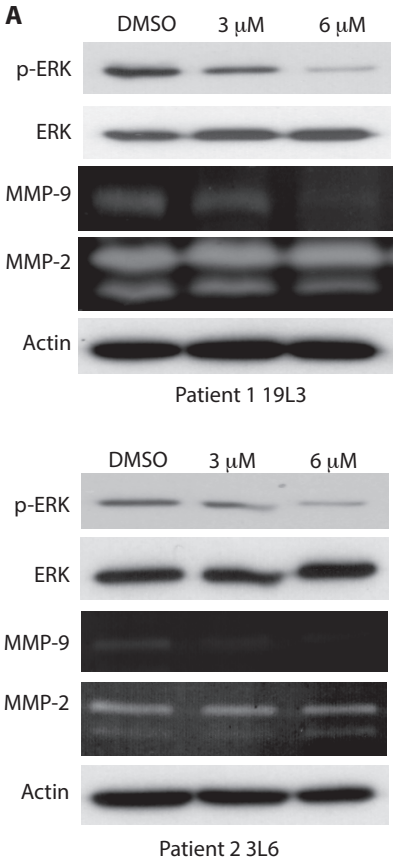

Figure S1. Generation and Characterization of iPSC Lines from Control and FTD Patients with *MAPT* Mutations (Related to Figure 1)

(A) Phase-contrast images (top panels, scale bar: 100 μm) and immunostaining of iPSC lines with different stem cell markers (scale bar: 50 μm).

(B) qRT-PCR analysis shows the expression levels of total and endogenous (Endo) reprogramming factors are similar, indicating silencing of the transgene. Values are mean ± S.D of three independent experiments.

(C) The karyotypes of newly generated iPSC lines are normal.

(D) *In vitro* spontaneous differentiation of different iPSC lines to demonstrate their pluripotency. Cells were immunostained with antibodies specific for markers of ectoderm (TUJ1), mesoderm (desmin), and endoderm (alpha-fetoprotein, AFP). Scale bar, 50 μm.

Figure S2. Characterization of Cortical Neurons Differentiated from Control and *MAPT* Mutant iPSCs (Related to Figure 1)

(A) Quantification of the percentage of MAP2-positive neurons in four-week-old neuron cultures Values are mean ± S.D of three experiments.

(B, C) Quantification of the percentage of VGLUT1-positive (glutametergic) neurons (B) and GABA-positive (GABAergic) neurons (C) among MAP2-positive neurons. No significant differences were found. Values are mean ± S.D of three independent experiments.

(D-H) Resting membrane potential (D), mean sEPSC amplitude (E), mean sEPSC frequency (F), rise time (G), and decay time constant (H) of human neurons differentiated from different iPSC lines. No significant differences were found. Values are mean ± SEM of two experiments and in each experiment, 7 neurons were recorded.

(I) The levels of secreted MMP-2 in 4-week-old control neurons and neurons with the progranulin S116X mutation are the same, as determined by Zymographic analysis. Cell lysates were analyzed by western blot with anti-actin antibody as a loading control.

(J) *MMP-2* and *MMP-9* mRNA levels in control and patient neurons measured by qRT-PCR. Values are mean ± SD of three experiments. ***: $p < 0.001$ by Student's t test.

Figure S3. Further Characterization of Human Cortical Neurons with *MAPT* Mutations (Related to Figure 2 and Figure 3)

(A) Lack of TUNEL labeling in GFAP-positive glial cells present in iPSC-derived cortical neuron cultures.

(B) Percentage of human neurons survival after treatment with DMSO or staurosporine (STS, 50 or 100 nM). Values are mean ± SD of three independent experiments.

(C) Percentage of human neurons survival after treatment with DMSO or rotenone (0.5 nM). Values are mean ± SD of three independent experiments.

(D) Neurotoxicity of MMP-2 and MMP-9 in iPSC-derived cortical neurons as assayed by TUNEL labeling. iPSC-derived cortical neurons were treated with 5 ug/ml MMP-2 and MMP-9 for 40 hours and then the extent of cell death was analyzed by TUNEL. Scale Bar: 10 μm.

(E) Quantification of the percentage of TUNEL-positive and MAP2-positive neurons from panel D. Values are mean ± SD of two independent experiments and in each experiment, 100 cells were counted for each condition.

(F) Quantification of 4R/3R *MAPT* mRNA ratios in control and patient cortical neurons as measured by RT-PCR. Values are mean ± SD from three experiments, by Student's t test.

(G) The 4R/3R *MAPT* mRNA ratio is not changed in *GRN* neurons compared with control neurons as measured by RT-PCR. Values are mean ± SD of three experiments, by Student's t test.

Figure S4. Regulation of MMP-9 Expression (Related to Figure 4)

(A) The level and activity of secreted MMP-9 in iPSC-derived cortical neurons of Patient 1 and Patient 2 directly correlates with the extent of ERK phosphorylation. Cortical neurons differentiated from patient iPSCs were treated with DMSO or different concentrations of the MEK inhibitor PD98059.

(B) Western blot analysis of human 3R WT or 3R tau-A152T in HEK293 cells.

(C) Zymographic analysis of secreted MMP-2 and MMP-9 in conditioned media from HEK293 cells expressing 3R WT and 3R tau-A152T, and western blot analysis of actin in the respective cell lysates.

(D) Western blot analysis of p-ERK and ERK in HEK293 cells expressing 3R WT or 3R tau-A152T.

EXPERIMENTAL PROCEDURES

Karyotyping Analysis

Standard G-banding analysis was performed by Cytogenetics Laboratory, University of Massachusetts Memorial Medical Center, Worcester, MA.

Neuronal Differentiation of iPSCs

IPSCs were differentiated into neurons as described (Almeida et al., 2012). Briefly, iPSC colonies were detached and grown in suspension for 6–8 days in iPSC medium without basic FGF to form embryoid bodies (EBs), which were seeded on poly-L-ornithine/laminin coated dish and maintained in neural induction medium to form rosettes. After 10 days, neuroepithelial cells in the rosettes were isolated from the surrounding cells with 0.2 mg/ml dispase. After 3–4 weeks, neurospheres were dissociated with accutase (Millipore), placed on glass coverslips coated with poly-D-lysine and laminin (BD), and cultured in neuron medium for 4 weeks. For spontaneous differentiation, EBs were obtained as described above, seeded on poly-L-ornithine/laminin-coated coverslips and cultured for 8 additional days. Cells migrating out of the EBs were fixed with 4% paraformaldehyde, permeabilized with 0.5% Triton X-100, immunostained for pluripotency markers, and analyzed by confocal microscopy.

Materials

The use of human skin biopsies was approved by the Institutional Review Board and Ethics Committee at the University of California, San Francisco (UCSF). Written informed consent was obtained in all cases. Experimental procedures are described in detail in Supplemental Methods.

Rapamycin, rotenone, and staurosporine were from Sigma. Horseradish peroxidase–conjugated secondary antibody was from Jackson ImmunoResearch Laboratories. PD98059, an MEK inhibitor, MMP-2 and MMP-9 inhibitors as well as recombinant MMP-2 and MMP-9 were from Calbiochem.

MTT Assay

Neurons used in the MTT assays were cultured in 24-well plates for 4 weeks. The MTT assays were done as recommended by the manufacturer (Promega).

Gene Expression Analysis

For mRNA expression analysis, total RNA was isolated with RNeasy kits (Qiagen), and 500 ng of RNA was reverse transcribed into cDNA with a Taqman reverse transcription reagent kit (Applied Biosystems). Quantitative RT-PCR was done with Taqman Gene Expression Master Mix and Taqman primers (for *OCT3/4*, *cMYC*, *SOX2, KLF4* and *GAPDH*) or SYBR Green PCR Master Mix (Applied Biosystems). The sequences of the primers used with SYBER Green are as following. 4R *MAPT*: forward - GAAGCTGGATCTTAGCAACG and reverse – GACGTGTTTGATATTATCCT. 3R *MAPT*: forward - AGGCGGGAAGGTGCAAATAG and reverse – TCCTGGTTTATGATGGATGTT. *GAPDH*: forward –TGCACCACCACCTGCTTAGC and reverse – GGCATGGACTGTGGTCATGAG. *MMP-2*: forward – ATGACAGCTGCACCACTGAG and reverse – TGATGTCATCCTGGGACAGA. *MMP-9*: forward - ATAAGGACGACGTGAATGGC and reverse – TCAAAGACCGAGTCCAGCTT. Ct values for each target gene were normalized to that of the *GAPDH*. The $2^{-\Delta\Delta Ct}$ method was used to determine the relative expression of each gene.

Immunofluorescence

Cells cultured on cover slips were fixed with 4% paraformaldehyde for 20 min and permeabilized with 0.5% Triton X-100 for 5 min. After incubation with 7% FBS in PBS for 1 h, cells were incubated with the primary and secondary antibodies in 7% FBS in PBS, and mounted on slides with Slow Fade Antifade reagent (containing DAPI). The primary antibodies used were mouse anti-OCT4 (1:100, Santa Cruz Biotechnology, sc-5279), mouse anti-SSEA4 (1:100, Abcam, ab16287), goat anti-NANOG (1:100, R&D Systems, AF1997), mouse anti-TRA-1-60 (1:100, Millipore, MAB4360), mouse anti-TRA-1-81 (1:100, Millipore, MAB4381), mouse anti-TUJ1 (1:200, Promega, G7121), rabbit anti-desmin (1:100, Thermo Scientific, RB-9014-PO), mouse anti-alpha-fetoprotein (1:200, R&D Systems, MAB1368), mouse anti-MAP2 (1:500, Sigma, M9942), rabbit anti-GABA (1:100, Sigma, A2052), and rabbit anti-VGLUT1 (1:500, Synaptic Systems, 135303). Slides were analyzed by confocal microscopy.

Electrophoresis and Immunoblotting

Electrophoresis and immunoblotting were done as described (Biswas et al., 2010). Briefly, proteins were subjected to SDS-PAGE and transferred to a PVDF membrane. The membrane was blocked and incubated with respective primary antibody at 4°C, overnight and with the secondary antibody at room temperature for 1 h. The primary antibodies used were mouse antibodies against MAP-2 (1:1000, Sigma, M9942), actin (1:2000, Sigma, A2228), and PSD95 (1:1000, Antibodies Inc., 75-028) and rabbit antibodies against tau (1:1000, Dako, A0024), ERK (1:1000, Cell Signaling, 4695), and p-ERK (1:1000, Cell Signaling, 9101). Proteins were visualized by enhanced chemiluminescence (Thermo Scientific).

Electrophysiology

Electrophysiological recordings were obtained from 4–5-week-old iPSC-derived neurons as described (Almeida et al., 2012). Action potentials were evoked with 200-msec depolarizing currents of 0–400 pA in 100-pA steps. AMPAR-mediated spontaneous excitatory postsynaptic currents (sEPSCs) were measured in whole-cell voltage-clamp mode with bath application of picrotoxin (0.1 mM, Sigma) and analyzed with Mini Analysis software (Synaptosoft). Results are shown as mean ± SEM. Statistical significance of changes in sEPSCs was determined by one-way ANOVA; $p < 0.05$ was considered statistically significant.

Measurement of MMP-2 and MMP-9 Activity by Zymography

MMP-2 and MMP-9 activities in conditioned medium were assayed by zymography as described (Biswas et al., 2010). Conditioned medium were subjected to SDS-PAGE with 0.3% Type-A gelatin (Sigma). The gels were washed, incubated for 18 h at 37°C in the reaction buffer (50 mM Tris-HCl, pH 7.4, 10 mM $CaCl_2$), stained with 0.1% Coomassie Brilliant Blue (CBB) for 1 hour, and destained in 50% H_2O, 40% methanol, and 10% acetic acid by volume. Finally, gel was sandwiched in two sheets of cellophane and air dried overnight. Activity of MMP-2 and MMP-9 was visualized as a transparent band against CBB background and quantified using ImageJ software (Biswas et al., 2010).

TUNEL assay

We performed TUNEL assay in one-month-old iPSC-derived cortical neurons from control and *MAPT* mutation subjects. In addition, we treated iPSC-derived cortical neurons with a combination of 5 μg/ml MMP-2/MMP-9 for 48 hours. We fix the neurons

from the two experiments with 4% PFA for 15 minutes and then we performed TUNEL assay with the Fluorescein in situ cell death detection kit (Roche). After we performed the TUNEL assay we did immunostaining with the mouse anti-MAP2 primary antibody (Sigma, 1:1000, M9942) followed by Alexa 568 anti-mouse secondary antibody (1:500, Thermo Scientific, A10037).

REFERENCES

Almeida, S., Zhang, Z., Coppola, G., Mao, W., Futai, K., Karydas, A., Geschwind, M.D., Tartaglia, M.C., Gao, F., Gianni, D. et al. (2012). Induced pluripotent stem cell models of progranulin-deficient frontotemporal dementia uncover specific reversible neuronal defects, *Cell Rep. 2*, 789–798.

Biswas, M.H., Du, C., Zhang, C., Straubhaar, J., Languino, L.R., and Balaji, K.C. (2010). Protein kinase D1 inhibits cell proliferation through matrix metalloproteinase-2 and matrix metalloproteinase-9 secretion in prostate cancer. *Cancer Res. 70*, 2095–2104.